Howard Hughes Medical Institute

Published as: *Nat Methods*. 2009 February ; 6(2): 131–133.

A bright and photostable photoconvertible fluorescent protein for fusion tags

Sean A. McKinney[1], **Christopher S. Murphy**[2], **Kristin L. Hazelwood**[2], **Michael W. Davidson**[2,#], and **Loren L. Looger**[1,#]

[1] Howard Hughes Medical Institute, Janelia Farm Research Campus, 19700 Helix Dr, Ashburn, VA 20147

[2] National High Magnetic Field Laboratory and Department of Biological Science, The Florida State University, 1800 E. Paul Dirac Dr., Tallahassee, Florida 32310

Abstract

Photoconvertible fluorescent proteins offer significant potential as tools for investigating dynamic processes in living cells and for emerging super-resolution microscopy techniques. Unfortunately, most probes in this class are hampered by oligomerization, small photon budgets, or poor photostability. Here we report an EosFP variant that functions well in a broad range of protein fusions for dynamic investigations, exhibits high photostability, and preserves the superior ~10-nm localization precision of its parent.

The recent development of superresolution imaging techniques has revolutionized the study of cellular ultrastructure with light microscopy. Photoactivated localization microscopy (PALM1, PALMIRA2, and FPALM3), reversible saturable optical fluorescence transitions (RESOLFT)4, and stochastic optical reconstruction microscopy (STORM)5, as well as related methodologies, including dual-color6, live-cell3, and 3D high-resolution imaging7, are among the unique innovations that have allowed modest fluorescence microscopes to reach far beyond the traditional diffraction limit. Despite their differences, these techniques share two critical enabling technologies: highly efficient detectors and fluorescent probes that photoswitch or photoconvert. Such probes allow the detection of single molecules over the background for high precision localization and the repetitive excitation and selective quenching of sub-diffraction annuli4.

[#]To whom correspondence should be addressed: L.L.L. : loogerl@janelia.hhmi.org, M.W.D. : davidson@magnet.fsu.edu.

AUTHOR CONTRIBUTIONS

L.L.L. designed mEos2 variants and S.M. generated and analyzed mEos2 variants and performed PALM imaging. M.W.D., K.L.H. and C.S.M. generated cloning vectors and fusion constructs, performed widefield, TIRF, and confocal microscopy, and conducted photobleaching experiments. S.M., M.W.D. and L.L.L. designed and planned the project and wrote the manuscript.

COMPETING FINANCIAL INTERESTS

The authors declare no competing financial interests.

Supplementary Text and Figures: Supplementary Figs. 1–13, Supplementary Tables 1–2, and Supplementary Methods

Targeting fluorescent probes to biological structures of interest can be performed using either labeled antibodies or fluorescent proteins (FPs) directly fused to signal peptides or specific target proteins. Immunofluorescence has the advantage of a larger probe palette from which to choose, including small molecules having larger photon budgets. High photon budgets are critical in localization techniques, including PALM and STORM, as the number of photons obtainable per activation cycle dictates the precision with which each fluorescent molecule is localized. Together with labeling density and background level, the photon budget determines a probe's resolving power. Organic dyes, including Cy5 and Cy7, typically feature localization precisions approaching a lower limit of four nm[5]. However, the harsh fixatives and detergent treatments required for immunofluorescence are undesirable. Furthermore, antibodies are limited in labeling density, often produce high levels of non-specific background signal, are seldom useful for live-cell imaging, and can artificially inflate feature size by virtue of their own non-trivial dimensions5.

For high resolution applications that must overcome such problems, FP fusions are currently the optimal solution. Unfortunately, the existing monomeric photoactivatable FPs (PaFPs) suffer from smaller photon budgets than synthetic dyes, leading to a substantial loss in localization precision. The green-to-red photoconverting FPs, Kaede and EosFP1, yield precisions almost as good as organic fluorophores, but exist in solution as tetrameric complexes, hampering their use as fusion partners. Tandem dimer (td) and monomeric (m) versions of EosFP8,9 have been engineered, but tdEos still fails to localize accurately in many standard targets, including tubulin, histones, intermediate filaments and gap junctions (Supplementary Fig. 1 online), while mEos does not mature at 37 °C and can only be successfully used at 30 °C where most mammalian cells may exhibit metabolic artifacts. Here we discuss the development of an mEosFP variant, dubbed mEos2, which folds efficiently at 37 °C and successfully labels targets that are intolerant of fusion to FP dimers and tandem dimers. This new variant preserves the superior localization precision of tdEos (~10 nm in 1D) and serves as a traditional green-to-red optical highlighter with comparable or superior maturation kinetics, acid sensitivity, photostability, and brightness to Dendra210, the only other monomeric highlighter in its class. mEos2 therefore enables super-resolution imaging of the most constructs at high localization precision, approaching that of organic fluorophores, but with the added advantage of excellent targeting arising from genetic encoding.

We pursued a strategy of side-chain grafting to stabilize the existing monomeric Eos variant (wtEosFP with V123T, T158H). EosFP is highly homologous to the green reversibly photoactivatable protein Dronpa11, which is bright, monomeric, and matures well at 37 °C. A structural alignment of EosFP (PDB 1ZUX) and Dronpa (PDB 2IE2) was created to identify divergent positions at which the Dronpa side-chain may contribute to thermal stability and monomeric character. To avoid disturbing the chromophore environment, our first approach was to mutate only sites on the barrel exterior, with an emphasis on positions where introducing a Dronpa residue might improve secondary structure preference or electrostatics (Supplementary Table 1 online), thus stabilizing the entire protein. Twenty positions were selected for mutagenesis, and three mutations (N11K, E70K, H74N) were found to rescue fluorescence at 37 °C in bacterial colonies. Surprisingly, these mutations are not found at either dimer-dimer interface and are solvent-exposed in the tetrameric crystal

structure. All three mutations were predicted to improve secondary structure preference (11, 70: β-strand; 74: Type I β-turn), and the mutations N11K and E70K to potentially improve electrostatics. Serendipitous mutation of His121 (the center of the A–C dimer-dimer interface) to Tyr rather than to the primer-encoded mutation Asp also aided 37 °C folding, potentially by simultaneously optimizing β-strand preference and disfavoring dimerization. These four mutations (dubbed mEos2) turned the original mEos8 into a functional green-to-red photoconvertible fluorescent protein at 37° C (Supplementary Fig. 2 online).

Purified mEos2 exhibits spectral properties, brightness, pK_a, photoconversion, contrast, and maturation properties nearly identical to the previous variants (wtEos, dEos (T158H), and tdEos, see Table 1 and Supplementary Figs. 3–6 online). To examine oligomeric character, we applied several techniques including gel filtration, homo-FRET12 (fluorescence resonance energy transfer), and hetero-FRET (Supplementary Figs. 7–8 online). Results suggested that mEos2 exhibited more dimeric character than its parent but further mutagenesis to remove this character proved detrimental in other ways (Supplementary Fig. 9 online). To determine whether this was a prohibitive problem, we fused mEos2 to targeting peptides and proteins known to exhibit artifacts for the dimeric and tandem-dimer species (Supplementary Figs. 1 and 10 online), and performed live-cell and PALM imaging.

The performance and photoconversion efficiency of all mEos2 fusions were monitored by observation of epithelial (HeLa) and fibroblast (gray fox lung) cells in transient transfections (Fig. 1 and Supplementary Figs. 1 and 10 online). N- and C-terminal mEos2 fusions localized as expected, and both the native and converted species were sufficiently photostable to gather time-lapse image sequences. mEos2 fused to histone H2B did not interfere with mitosis (Fig. 1g–j and Supplementary Fig. 10m-q online) and photoconversion was used to dynamically monitor cell division, mitochondrial fusion, and gap junction plaque behavior (Fig. 1a–f). Fusions of mEos2 with signal peptides and targeting proteins confirmed expected localization patterns (Supplementary Fig. 10 online) in focal adhesions (paxillin and zyxin), Golgi complex, clathrin-coated pits, intermediate filaments (keratin and vimentin), nuclear envelope (lamin B1) and microtubules (tubulin and EB3). In contrast, many tdEos fusions gave rise to localization defects or aggregation, including those targeting EB3, tubulin, connexins, histones, and intermediate filaments. These results suggest that the despite its residual weak dimericity at high concentrations, mEos2 is an excellent fusion partner for biological imaging, even in difficult fusions (although there may remain untested fusion partners for which the residual dimeric character might prove disruptive).

Widefield (using metal halide arc lamp illumination) and laser scanning confocal microscopy photobleaching kinetics (Table 1 and Supplementary Fig. 11 online) revealed that the green species of the optical highlighters in this study (mPA-GFP, Dendra2, wtEos, dEos, tdEos, and mEos2) exhibited photostabilities of ~25% or less that of mEGFP. In contrast, photostability of the photoconverted (red) species was higher than that of mCherry with metal halide illumination, but less than or equal to mCherry under laser illumination. The mEos2 red species exhibited the highest level of photostability in all of the monomer-like highlighter FPs examined under laser illumination (and close to that of the tandem dimer), which is the primary imaging mode for tracking dynamic events in living cells.

Similar photobleaching rates were observed for tdEos, Dendra2 and mEos2, however photobleaching is only one of many components causing bright-to-dark transitions of fluorophores at the single molecule level. Therefore, to ensure that mEos2 maintained the ~10 nm localization precision of dEos and tdEos, we conducted PALM imaging on fusions that failed to localize well with the latter variants, including EB3, vimentin, and keratin. Individual Eos molecules fused to the target protein were converted to the red species sparsely, but continuously, using a 405-nm laser while simultaneously performing total internal reflection fluorescence (TIRF) imaging with a 561-nm laser. PALM analysis was performed as described1. The PALM images obtained with mEos2 revealed high resolution structures not visible in diffraction-limited imaging (Fig. 2). Localization precisions were comparable to those for tdEos (11 nm in cells) and two to four times more precise than Dendra2 (23 nm), Dronpa (26 nm^6), PS-CFP2 (27 nm^6), and mPA-GFP (41 nm^3) (Supplementary Table 2 and Supplementary Figs. 12–13 online). Fluorophore molecular densities, the other barrier in determining probe resolution due to the Nyquist criterion (Supplementary Table 2 online), were comparable in feature rich areas for Dendra2-keratin and mEos2-keratin (4,800 and 6,500 molecules/μm^2 respectively) but sufficiently small to make filtering of poorly localizing molecules costly in terms of final image resolution.

In summary, mEos2 is an excellent candidate to replace Dendra2 and tdEos for dynamic investigations in live-cell imaging and for super-resolution imaging with PALM and related techniques. The excellent photostability exhibited by the photoconverted species of mEos2 enables long-term imaging, and the weakly dimeric character coupled to the exceptional targeting allow mEos2 to be used in fusions that are problematic with tdEos or dEos. Furthermore, the localization precision of mEos2 is two-fold greater than that of Dendra2 (or any other monomer), making it one of the most useful genetically encoded PALM probes reported to date. Highly fusible, high-contrast PALM fluorescent probes, such as mEos2, should help to unravel the superstructures of difficult protein complexes.

Supplementary Material

Refer to Web version on PubMed Central for supplementary material.

Acknowledgments

We thank Helen White and Sarah Winfrey for cell cultures and transfections and Eric Betzig and Hari Shroff (Janelia Farm Research Campus) for PALM imaging help and for their analysis software. We are grateful to Ericka Ramko and Corey Wilson (National High Magnetic Field Laboratory) for technical assistance with fusion vector construction. Vector DNA sequences were provided by the Florida State University Bioanalytical and Molecular DNA Sequencing Facility or the Janelia Farm Research Campus Molecular Biology Shared Resource.

References

1. Betzig E, et al. Science. 2006; 313:1642–1645. [PubMed: 16902090]
2. Egner A, et al. Biophys J. 2007; 93:3285–3290. [PubMed: 17660318]
3. Hess ST, et al. Proc Natl Acad Sci USA. 2007; 104:17370–17375. [PubMed: 17959773]
4. Hofmann M, Eggeling C, Jakobs S, Hell SW. Proc Natl Acad Sci USA. 2005; 102:17565–17569. [PubMed: 16314572]
5. Bates M, Huang B, Dempsey GT, Zhuang X. Science. 2007; 317:1749–1753. [PubMed: 17702910]
6. Shroff H, et al. Proc Natl Acad Sci USA. 2007; 104:20308–20313. [PubMed: 18077327]

7. Huang B, Wang W, Bates M, Zhuang X. Science. 2008; 319:810–813. [PubMed: 18174397]
8. Wiedenmann J, et al. Proc Natl Acad Sci USA. 2004; 101:15905–15910. [PubMed: 15505211]
9. Nienhaus GU, et al. Photochem Photobiol. 2006; 82:351–358. [PubMed: 16613485]
10. Gurskaya NG, et al. Nat Biotechnol. 2006; 24:461–465. [PubMed: 16550175]
11. Ando R, Mizuno H, Miyawaki A. Science. 2004; 306:1370–1373. [PubMed: 15550670]
12. Gautier I, et al. Biophys J. 2001; 80:3000–3008. [PubMed: 11371472]
13. Shaner NC, et al. Nat Methods. 2008
14. Patterson GH, Lippincott-Schwartz J. Science. 2002; 297:1873–1877. [PubMed: 12228718]
15. Tsutsui H, et al. EMBO Rep. 2005; 6:233–238. [PubMed: 15731765]

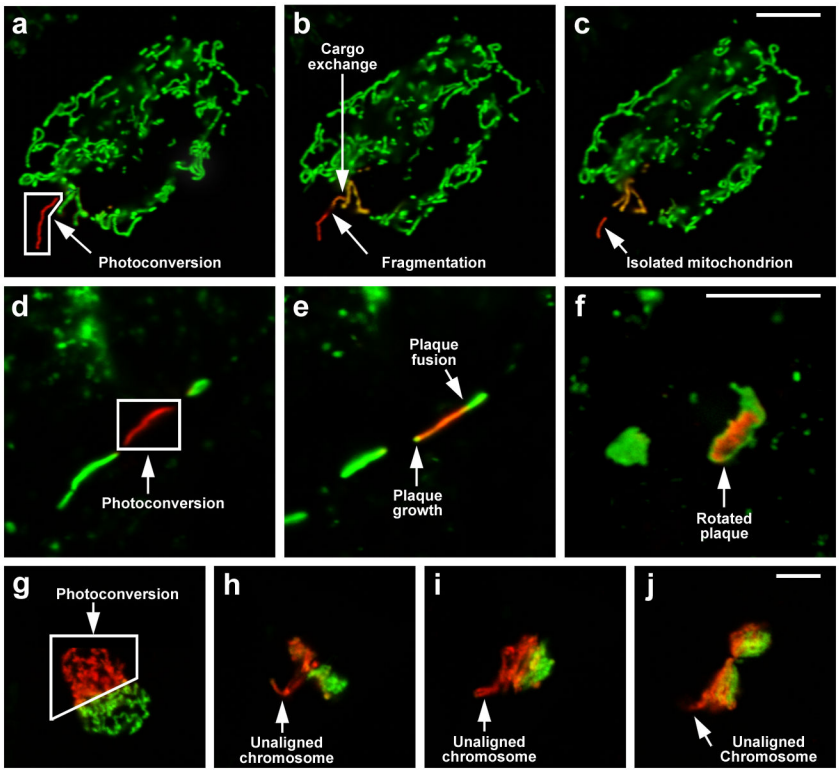

Figure 1. Tracking dynamics in live cells with mEos2 fusions

(**a**)–(**c**): Mitochondrial dynamics observed by photoconversion of a single mitochondrion (red) in adherent HeLa epithelial cells expressing mEos2–7AA linker-mitochondria. (**a**) Region of interest (white polygon) is illuminated at 405 nm for 5 sec, *t* = 0; (**b**) the photoconverted mitochondrion fragments and exchanges cargo with an adjacent mitochondrion, *t* = 5 min; (**c**) a portion of the fragmented mitochondrion condenses and migrates away from neighbors, *t* = 15 min. (**d**)–(**f**): Gap junction plaque (GJs) dynamics in HeLa cells expressing the connexin fusion mEos2–7AA linker-Cx43. (**d**) The central GJ plaque in a trio is photoconverted to red (white box), *t* = 0; (**e**) Fusion of a native plaque (green) to the photoconverted plaque, as well as new plaque growth are observed, *t* = 70 min; (**f**) Rotated plaque reveals photoconverted area surrounded by unconverted fusion and new growth, *t* = 120 min. (**g**)–(**j**): Observing mitosis in pig kidney cells (LLC-PK1 line) with the histone fusion mEos2–6AA linker-H2B. (**g**) Approximately half of the condensed chromatin in a prophase cell is photoconverted (white polygon) for 3 sec, *t* = 0; (**h**) Alignment at the spindle shows clear segregation between the native and photoconverted chromatin. Note the unaligned chromosome that serves as a reference point, *t* = 40 min; (**i**) In early anaphase, the unaligned chromosome is still present, *t* = 70 min; (**j**) in telophase, the daughter nuclei begin to form, *t* = 170 min. Scale bars represent 10 μm.

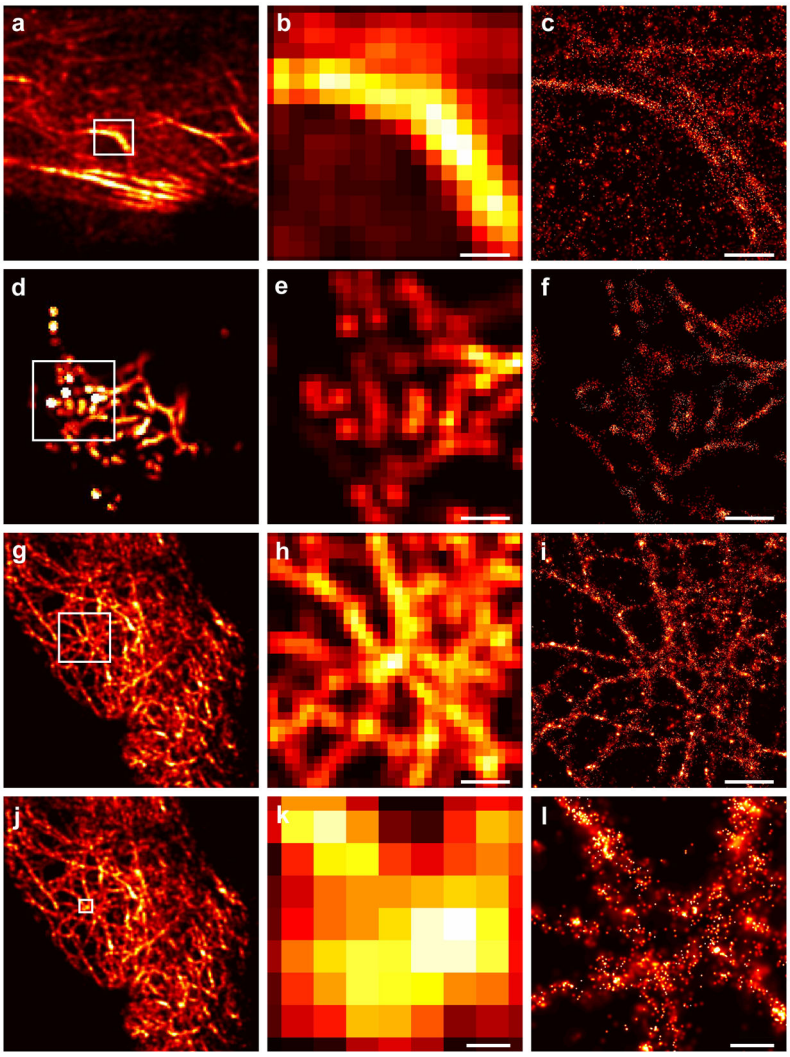

Figure 2. PALM Images of mEos2 fusions

(**a–c**) mEos2 fusions to microtubule end-binding protein EB3 in a highly expressing cell decorate microtubule filaments. (**a**) Widefield TIRF image showing the edge in a HeLa cell and area of interest. (**b**) TIRF-resolution image in area of interest (scale bar 500 nm). (**c**) The same region of interest in PALM; note the emergence of fibers that are irresolvable in the standard TIRF image. (**d–f**) mEos2 fused to vimentin. (**d**) Widefield TIRF image of the network close to the surface and region of interest. (**e**) TIRF resolution image in region of interest (scale bar 1 μm). (**f**) PALM image of same region. Note what appears to be an intersection of three fibers in the bottom right of the TIRF image (**e**) is shown to not be. (**g–l**) mEos2 fusions to keratin. (**g, j**) Whole cell TIRF images with areas of interest, (**h–i**) and (**k–l**), respectively. (**h, k**) Diffraction limited images of the adjacent regions of interest (scale bars of 1 μm and 200 nm, respectively). (**i**) The corresponding PALM image for (**h**) details the intricate network of keratin fibers. (**l**) The simple blob that appears in (**k**) is resolved into an intersection of fibers, with a large dark area in the center of the hub that appears as a bright blur in the diffraction limited image. Features of ~50nm are resolved despite

substantially higher probe localization, a similar lower limit on feature sizes has been exhibited elsewhere with other probes3,5.

Table 1

Key characteristics of mEos2 in comparison with control (mEGFP and mCherry) and other photoconvertible fluorescent proteins

Fluorescent Protein	Ex[a] (nm)	Em[a] (nm)	QY[a]	EC[a] ($M^{-1}cm^{-1}$)	Brightness[b]	pKa[a]	Photostability[d] (Widefield)	Photostability[d] (Confocal)	Ref
mEGFP	484	507	0.60	56,000	34	6.0	202	5,010	13
mCherry	587	610	0.22	72,000	16	< 4.5	168	2,770	13
mPA-GFP (G)	504	517	0.79	17,400	14	4.5	24	710	14
wtEos (G)	506	516	0.70	72,000	50	5.7	58	510	8
wtEos (R)	571	581	0.55	41,000	23	-	489	1,890	8
dEos (G)	506	516	0.66 (0.84)[c]	84,000 (57,000)[c]	55 (48)[c]	5.7	49	350	8
dEos (R)	569	581	0.60 (0.58)[c]	33,000 (49,000)[c]	20 (28)[c]	-	485	3,130	8
tdEos (G)	506	516	0.66 (0.91)[c]	84,000 (65,000)[c]	55 (59)[c]	5.7	47	430	9
tdEos (R)	569	581	0.60 0.62)[c]	33,000 (48,000)[c]	20 (30)[c]	-	380	2,730	9
mEos2 (G)	506	519	(0.84)[c]	(56,000)[c]	47	5.6	42	240	this work
mEos2 (R)	573	584	(0.66)[c]	(46,000)[c]	30	6.4	323	2,700	this work
Dendra2 (G)	490	507	0.50	45,000	23	6.6	45	260	10
Dendra2 (R)	553	573	0.55	35,000	19	6.9	378	2,420	10
Kaede (G)	508	518	0.88	98,800	87	5.6	53	990	15
Kaede (R)	572	580	0.33	60,400	20	5.6	386	1,660	15

[a] Literature values unless indicated otherwise.

[b] Brightness is calculated as a product of molar extinction coefficient (EC) and fluorescence quantum yield (QY) in $mM \cdot cm^{-1}$ and represents only an idealized maximum photon emission rate devoid of saturation and other intermittencies.

[c] Values obtained by our lab at the same time as mEos2 show similar green-form brightness, but different EC and QY, compared to published values. All forms of Eos (including mEos2) showed similar values to one another.

[d] Time to bleach to 50% initial fluorescence emission rate under conditions calculated to begin with 1000 photons/second/molecule (see Supplementary Methods online).